IEEE Access
Multidisciplinary | Rapid Review | Open Access Journal

Received February 14, 2022, accepted March 8, 2022, date of publication March 14, 2022, date of current version March 25, 2022.

Digital Object Identifier 10.1109/ACCESS.2022.3159623

Tracking of Radar Targets With In-Band Wireless Communication Interference in RadComm Spectrum Sharing

GUNNERY SRINATH, (Graduate Student Member, IEEE), BETHI PARDHASARADHI, (Member, IEEE), PRASHANTHA KUMAR H., AND PATHIPATI SRIHARI, (Senior Member, IEEE)

Department of ECE, National Institute of Technology Karnataka, Surathkal, Mangalore 575025, India

Corresponding author: Pathipati Srihari (srihari@nitk.edu.in)

This work was supported in part by the Visvesvaraya Ph.D. Scheme of the Ministry of Electronics and Information Technology, Government of India, being implemented by Digital India Corporation; and in part by the National Institute of Technology Karnataka, Surathkal, University Grants Commission of India.

ABSTRACT Radar and communication system (RadComm) spectrum sharing has received considerable attention from the research community in recent years. This paper considers the distributed radars present in the surveillance region with multiple in-band wireless communication transmitters (IWCTs). A new measurement model is proposed by considering both radar returns and returns due to IWCTs. The tracking performance is evaluated using the global nearest neighbor (GNN) tracker with an extended Kalman filter (EKF) for the received measurement set. A single radar case is considered, where near geometry scenario (IWCTs are placed near the radar and target) and far-geometry scenario (IWCTs are placed far from the radar and target) are considered to evaluate the tracking performance. It is observed that a large number of tracks are resulted due to IWCTs, and identifying the actual target track is ambiguous in a single radar case. Therefore, in the second case, multiple radars are placed to investigate the problem comprehensively. The track-to-track association (T2TA) is performed to identify the true target track on multiple tracks produced owing to the presence of IWCTs and the resulting tracks from all radars pertaining to the true targets. Once the true target tracks from each radar are identified, using the T2TA, the track-to-track fusion (T2TF) is carried out to improve the estimates of the true target. The simulation results are quantified with position root mean square error (PRMSE). The posterior Cramer–Rao lower bounds (PCRLBs) quantifying the achievable estimation accuracies are also presented. The simulation results reveal that the association and fusion of tracks from multiple radars identify the true target track with good accuracy and overcome the inability to determine the true track, as in the case of a single radar. Further, the results disclose that, as the number of radars increases, the T2TA and fusion improved the PRMSE.

INDEX TERMS Communication system, in-band interference, radar system, spectrum sharing, target tracking, association, fusion.

I. INTRODUCTION

The available spectrum is becoming congested [1] owing to rapid growth in the usage of wireless devices [2]. Because of this, wireless users' accommodation and providing good quality of service, as per their requirements, are becoming extremely difficult. As a result, the radar and communication system (RadComm) spectrum sharing has been paying attention over the past years [3]. Sharing the underutilized, permanently allocated, and a large amount of available radar bandwidth with the communication systems serves the wireless user demands and improves the effective utilization of the spectrum [4]. The RadComm spectrum sharing research is broadly categorized into two sub-topics: radar-communication coexistence (RCC) and dual-functional radar-communication (DFRC) system design. In RCC, the

The associate editor coordinating the review of this manuscript and approving it for publication was Mehdi Hosseinzadeh.

radar and communication systems work independently in a cooperative/ non-cooperative manner within the same frequency band. As these systems operate in the same frequency band, they cause interference to each other. On the other hand, in DRFC systems, a single system possesses both radar and communication system functionalities. Since radar and communication are accommodated within the same system, interference occurs. The first category of research aims to develop efficient interference management techniques so that the two systems can operate without undue interference. Alternatively, DFRC techniques focus on designing joint systems that simultaneously perform wireless communication and remote sensing. This benefits both sensing and signaling operations via real-time cooperation, de-congests the RF environment, and allows a single hardware platform for both functionalities.

A. RELATED WORKS

A comprehensive survey of radar and communication system spectrum sharing is provided in [3], [5], and [6]. The effect of interference in RCC, from a communication system perspective, is presented in [7]. Besides, in [8] it is assumed that the radar and communication system are located apart; the target time delay parameter is estimated by designing the optimal waveform for the radar system, with a constraint on Cramér–Rao Bound (CRB). Also, it is demonstrated that using additional constraints like transmitted power and subcarrier power ratio (SPR) while designing the optimized radar waveform reduces delay ambiguities. Further, [9] and [10] discuss using a single radar waveform that can embed the communication symbols for communication purposes and vice-versa. Especially in [10], a novel continuous phase modulation (CPM) based information-bearing waveform is proposed, without degrading the spectral characteristics, for improving radar target detection and maintaining high power with constant envelope constraint for long-range target visibility. In another communication, the single-input single-output (SISO) and multi-input multi-output (MIMO)-based architectures, for the joint RadComm, have been investigated [11]. The system design in [11] is based on the maximization of signal-to-interference-plus-noise ratio (SINR) at the radar receiver. Further, in [11], by maintaining the achieved SINR at the radar receiver, the maximization of communication rate constraint is additionally imposed for communication purposes. Authors in [12] have derived the novel estimation and information rate bounds for a DFRC system, and its performance is evaluated using the derived bounds. Besides, the extension of joint performance bounds with clutter is presented in [13]. In addition, the same performance bounds have been extended for the case of frequency-modulated continuous-wave (FMCW) radar [14]. Further, in the recent contribution [15], a joint RadComm is considered, where overall bandwidth is shared among the radar and communication system in an independent coexistence, and a partial band coexistence manner is presented.

Moreover, in [15], the performance is analyzed in terms of mutual information (MI) and communication data rate. Furthermore, the statistical model for in-band wireless communication interference and its effect on the adaptive threshold-based detector at the radar receiver is analyzed in [16]. The results in [16] show that interference follows non-Gaussian statistics, and the detection of targets using a cell averaging detector provides inadequate performance in identifying the target and demands for alternative and efficient detection schemes. A novel whitening filter followed by matched filter detector is proposed to detect the radar targets in the presence of in-band communication interference [17]. The DFRC system design for automotive applications has been studied in [18], [19]. The joint transmit waveform design and receiver design for the DFRC system are studied in [20]. In contrast to other works, in [20], the radar performance is optimized without knowing a predetermined radar beam pattern. In [21], the performance of the DFRC systems is analyzed in terms of radar mutual information (RMI) and communication data rate (CDR) for radar and communication systems. The analysis assumes that the DFRC system transmits/receives the radar and communication signals on the isolated bands (isolation-based scheme) and the same band (sharing-based scheme). Further, in [21] for an isolated-based scheme, the RMI/CDR maximization of the DFRC system is solved independently with the constraint on optimal power allocation solutions. At the same time, the joint maximization of RMI/CDR for the DFRC system is solved for a sharing-based scheme [21]. An ultra-wideband chaotic radar with wireless synchronization command is proposed in [22] for target localization and tracking. In [23], considering the RadComm spectrum sharing in a cooperative and non-cooperative manner, a thorough literature survey and future research directions are presented. The above literature review reveals that RadComm spectrum sharing works primarily focused on detection, waveform design perspective, and deriving the bounds point of view.

Target tracking is an essential requirement, where one or more sensors are employed to estimate the time-varying kinematics of targets within the given surveillance region. The measurements are from diverse sources such as the targets of interest, clutter, etc. The main objective of target tracking is to partition the received measurements and form tracks for the targets of interest by estimating parameters like position, velocity, acceleration, turn, intensity, etc. Target tracking typically contains filtering, data association, and track management. The Kalman filter (KF) provides an optimal estimate under the considerations of linearity and Gaussian distribution [24]. Whereas, converted Kalman filter, extended Kalman filter (EKF), cubature Kalman filter (CKF), unscented Kalman filter (UKF), and particle Kalman filter (PKF), Interactive multiple models (IMM), etc.. [25] are widely used to address the non-linearity. While it comes to the data association, nearest neighbor (NN) and global nearest neighbor (GNN) are traditional associations methods, which use a single measurement out of all available measurements

falling within the validation gate [26]. In contrast, the Probabilistic Data Association (PDA) method applies the weighted sum of all the measurements within the validation gate [27]. The optimal approach for target tracking was demonstrated using a Multiple hypothesis tracker (MHT) under the assumption of propagating all the hypotheses into tracks [28]. The logic-based track maintenance and quality-based track maintenance are popularly used for track management [29].

The target tracking can be performed by using single/multiple sensors either in centralized or distributed configurations [25]. In distributed target tracking, track-to-track association (T2TA) is an important block to distinguish and assign the tuples corresponding to the targets [30]. The tuples of tracks reported by the T2TA module are fused to attain the global estimates. Generally, Track-to-tack fusion (T2TF) is classified into correlation free and correlation-based fusion approaches [31]. The correlation-based fusion technique requires the exact cross covariances among the local tracks of the same target. Hence, a large amount of information exchange is required between the fusion center (FC) and the local trackers, which makes this method realizable for practical scenarios [32]. Theoretically, information matrix fusion (IMF) or centralized tracking provides an optimal estimate/fused track [25]. The correlation-free fusion-based algorithms work independently of cross covariances, which allow the fusion to be performed at any local tracker without the participation of the fusion center. The ellipsoidal intersect (EI) [33], covariance intersect (CI) [34], sampling covariance intersect (SCI) [35] etc., comes under the correlation free fusion methods. Besides, these three methods provide the fused estimate by approximating the intersection region of individual ellipsoids. Among them, the EI, CI works better for two sensor-based fusion. On the other hand, the SCI has more flexibility to fuse the data from more sensors.

Based on the above critical literature review, in RadComm spectrum sharing systems, the target tracking-based contributions are hardly reported. There are insignificant research works that focus on target tracking and data fusion. Therefore, there is a need to conduct research in this direction, which motivates the proposed research investigation. As target tracking is an essential aspect for estimating the target dynamics, this paper considers the effect of in-band wireless communication interference on target tracking in RadComm spectrum sharing. A new measurement model is proposed for multiple radars surrounded by the multiple IWCTs scenario. This new measurement model considers all the measurements evolved due to radar, IWCTs, and false alarms. This paper proposes to use distributed radars, with the local tracker, by considering all the available measurements and performing target tracking using the Extended Kalman filter and Global nearest neighbor (GNN) association. The work suggests considering all the local tracks evolved from all sensors and performing an S-D assignment-based track-to-track association (T2TA) to identify the tracks associated with the radar targets rather than falsified target evolved due to the presence of IWCTs. Once the actual tracks are separated from all the grown tracks using T2TA, the track-to-track fusion (T2TF) is performed to achieve the global tracks. Here, the correlation-free fusion algorithms (ellipsoidal intersect (EI), covariance intersect (CI), and sampling covariance intersect (SCI)) is used for fusion. The key contributions of the paper are

1) A new measurement model is proposed for multiple radars surrounded by the multiple IWCTs scenario and performed distributed tracking.
2) An S-D assignment-based track-to-track association (T2TA) is formulated to identify the actual target tracks.
3) The track-to-track fusion (T2TF) is performed to improve the tracking performance.

The rest of the paper is organized as follows. Section II outlines the problem formulation. In Section III, the measurement model and the target tracking algorithm considered for the analysis is presented. Track to track association and fusion are incorporated in Section IV. The PCRLB calculations are presented in Section V. The results and discussion are provided in Section VI. Finally, the concluding remarks are given Section VII.

II. PROBLEM FORMULATION

A RadComm spectrum sharing scenario is considered, where N mono-static radars are present over a surveillance region to detect the radar targets and are surrounded by M in-band wireless communication transmitters (IWCTs). The radar static locations are $\{\mathbf{x}_n^r\}_{n=1}^N$ and IWCTs locations are $\{\mathbf{x}_m^c\}_{m=1}^M$, as shown in Figure 1. Because of the in-band operation of IWCTs, the radar system receives the target echoes from both the mono-static emission and in-band transmitter emission. Also, it receives direct path signals from wireless transmitters. We refer to these two directions of signal reception as surveillance channels and reference channels. In Figure 1, the thick lines and dotted lines indicate surveillance and reference channels, respectively. Therefore, the received signal at the n^{th} radar receiver, for a given target surrounded by M IWCTs, is given by

$$s_r^n(t) = \begin{cases} \sum_{n=1}^{N} s_{r_n}(t) + \sum_{m=1}^{M} s_{r_{cm}}(t) + n(t) = s_{r_{sur_n}}(t) \\ \sum_{m=1}^{M} s_{r_{c_{dm}}}(t) + n(t) = s_{r_{ref_n}}(t). \end{cases} \tag{1}$$

Here $s_{r_n}(t)$ is the target return from n^{th} radar, $s_{r_{cm}}(t)$ is the target echo from the m^{th} surrounding communication system transmitter. In addition, $s_{r_{c_{dm}}}(t)$ is the direct path signal from the surrounding m^{th} IWCT and $n(t)$ is the receiver noise. Further, $s_{r_{sur_n}}(t)$, $s_{r_{ref_n}}(t)$ are the received signals received through surveillance and reference channel of the n^{th} radar, respectively.

For simplicity, assume one radar and one in-band transmitter in a clean environment (unity target detection probability, zero false alarms). The received signal is processed with

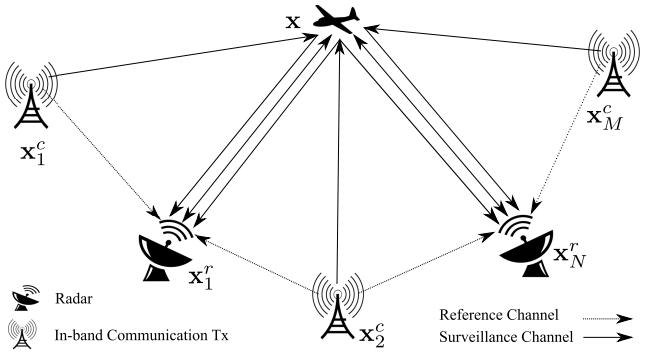

FIGURE 1. System model illustrating RadComm spectrum sharing scenario.

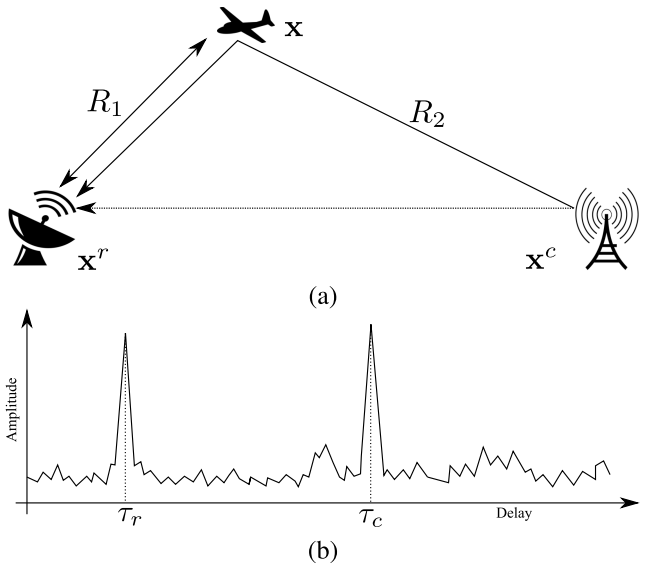

FIGURE 2. Reduced system model with single in-band transmitter and the corresponding correlator output.

matched filter-based receiver [36]. The correlator output at the receiver depicts peaks at τ_r and τ_c, as shown in Figure 2b. It is because of the fact that the radar receiver correlates the received signals with its own transmitted signal and the direct path reference signals received from IWCTs. The τ_r is the delay due to radar only return, and the corresponding range is given by $\frac{c\tau_r}{2}$. In contrast, τ_c is due to communication signal return. However, the radar assumes it as its own return (because of inadequate knowledge about the presence of IWCTs), and the corresponding range is calculated as $\frac{c\tau_c}{2}$. Here, c is the speed of light in free space. The corresponding geometry is depicted in Figure 2a. Hence, the presence of a single target and a single in-band transmitter in a given region results in two measurements at the radar receiver. As shown in Figure 2a, if R_1 is the distance from radar ($\mathbf{x}^r$) to a target ($\mathbf{x}$), R_2 is the distance between the in-band wireless transmitter ($\mathbf{x}^c$) to target ($\mathbf{x}$), the τ_r and τ_c is given by

$$\tau_r = \frac{2R_1}{c} \quad \text{and}$$

$$\tau_c = \frac{(R_1 + R_2)}{c}, \tag{2}$$

respectively. It is assumed that radar also receives the bearing information, apart from the range information. However, the bearing information is the same for both cases. Since the direction of arrival of target returns are in the same direction.

Even though a single target is present in this scenario, the radar receives multiple measurements owing to IWCTs. Hence, there is a need to distinguish true target measurements from all the evolved measurements. This paper proposes to analyze the target tracking performance for the above-stated problem.

III. TARGET TRACKING

This section briefly discusses the measurement model, state model, and GNN tracker for evaluating tracking performance in RadComm spectrum sharing scenario. The radars work in distributed configuration and estimate the target kinematics using a local tracker. This section presents the tracking of n^{th} radar. However, the subscript n has been removed for better reading and deriving the generalized mathematical model.

A. MEASUREMENT MODEL

The measurement set received by the radar n at time k is

$$\mathbf{Z}(k) = \{z_i(k)\}_{i=1}^{q_k}. \tag{3}$$

The measurement set obtained at k^{th} time instant contains q_k measurements, in which n_k measurements corresponds to mono-static radar, m_k measurements corresponds to IWCT, and e_k false alarms. i.e., $q_k = n_k + m_k + e_k$. In the given surveillance, the presence of $\{\mathbf{x}_l^t\}_{l=1}^{L}$ true targets, and $\{\mathbf{x}_m^c\}_{m=1}^{M}$ IWCTs result in $L + L \times M$ measurements at each radar. The measurement model is given by

$$z_i(k) = h(X(k)) + w_i(k), \tag{4}$$

where $X(\cdot)$ represents the state vector of the target at scan k, $h(\cdot)$ is a non-linear function to map the state space in polar to the Cartesian state.

The measurements not only pertain to the target originated but also the false alarms. These false alarms are independent and follow Poisson distribution, given by

$$\mathcal{P}(e) = \exp(-E)\frac{(E)^e}{e!}, \tag{5}$$

where E is the number of cells under consideration over a volume V. The spatial density of false alarm is given by

$$\lambda = \frac{E}{V}. \tag{6}$$

The probability of having q_k measurements in a given volume V is

$$p(q_k) = \begin{cases} (1 - p_D)\mathcal{P}(0); & q_k = 0, \\ (1 - p_D)\mathcal{P}(q_k) + p_D\mathcal{P}(q_k - 1); & q_k > 0, \end{cases} \tag{7}$$

where p_D is the target probability detection.

The measurements that originate at n^{th} mono-static radar, due to the presence of L targets, and M surrounding IWCTs, is represented as

$$\mathbf{Z}(k)=\begin{cases}\begin{bmatrix}R_n^l+\mathcal{N}(0,\sigma_r^2)\\ \theta+\mathcal{N}(0,\sigma_\theta^2)\end{bmatrix}; & l=1,\cdots L;\\ & \text{radar return}\\ \begin{bmatrix}R_n^l+R_m^l+\mathcal{N}(0,\sigma_r^2)\\ \theta+\mathcal{N}(0,\sigma_\theta^2)\end{bmatrix}; & l=1,\cdots L,\\ & m=1.\cdots M;\\ & \text{due to in-band Tx}\\ e_k; & \text{false alarms}\end{cases} \tag{8}$$

Here, R_n^l is the Euclidean distance between radar location $\mathbf{x}_n^r$ and target location $\mathbf{x}_l^t$, and is given by

$$R_n^l=\sqrt{(x_n^r-x_l^t)^2+(y_n^r-y_l^t)^2}. \tag{9}$$

Similarly, the R_m^l is the Euclidean distance between the target $\mathbf{x}_l^t$ and in-band wireless transmitter $\mathbf{x}_m^c$, is given by

$$R_m^l=\sqrt{(x_m^c-x_l^t)^2+(y_m^c-y_l^t)^2}. \tag{10}$$

Here, θ is the same for radar and in-band returns. Since the direction of arrival of target returns are in the same direction. It is given by

$$\theta=\arctan\left(\frac{y_n^r-y_l^t}{x_n^r-x_l^t}\right). \tag{11}$$

The noise components in range and azimuth are mutually independent and follow white Gaussian distribution with mean zero and standard deviation σ_r and σ_θ, respectively. The stacked vector of range and azimuth measurement noises is $w(k)$ and its measurement noise covariance is given by

$$R(k)=\mathbb{E}\{w(k)w(k)'\}, \tag{12}$$

where $\mathbb{E}$ represents the expectation operator, $[.]'$ represents the transpose operation.

B. STATE MODEL

The state transition model follows additive white Gaussian noise [24] and is given by

$$X(k+1)=F(k)X(k)+v(k), \tag{13}$$

Here, $X(k)$ is the four dimensional state vector constructed by stacking the position and velocity of the target as $[x(k),\dot{x}(k),y(k),\dot{y}(k)]'$, $v(k)$ is a zero-mean white Gaussian process noise vector and its covariance matrix is

$$Q(k)=\mathbb{E}[v(k)v(k)']. \tag{14}$$

The $F(k)$ represents the state transition matrix; for the constant velocity (CV) model, the state transition is given by

$$F(k)=\begin{bmatrix}1&t_s&0&0\\0&1&0&0\\0&0&1&t_s\\0&0&0&1\end{bmatrix}, \tag{15}$$

where t_s is a sampling time.

C. FILTERING

The filter involves three main steps, namely predictions, gain calculation, and updation. The predicted state and covariance are given by

$$\hat{X}(k+1|k)=F\hat{X}(k|k)\quad\text{and} \tag{16}$$

$$P(k+1|k)=FP(k|k)F'+Q(k), \tag{17}$$

respectively. The measurement prediction is represented as

$$\hat{z}(k+1)=H\hat{X}(k+1|k). \tag{18}$$

Here, H is a linearized form of measurement transition matrix and is given by

$$H\approx\begin{bmatrix}\frac{\partial r}{\partial x}&\frac{\partial r}{\partial \dot{x}}&\frac{\partial r}{\partial y}&\frac{\partial r}{\partial \dot{y}}\\ \frac{\partial \theta}{\partial x}&\frac{\partial \theta}{\partial \dot{x}}&\frac{\partial \theta}{\partial y}&\frac{\partial \theta}{\partial \dot{y}}\end{bmatrix}. \tag{19}$$

The innovation is given by

$$\gamma=z(k+1)-\hat{z}(k+1|k), \tag{20}$$

where $\hat{z}(k+1|k)$ is determined by the data association module.

The Kalman gain K is computed as

$$K(k+1)=P(k+1/k)H(k+1)'\left[H(k+1)P(k+1/k)H(k+1)'+R\right]^{-1}, \tag{21}$$

where R is the measurement covariance matrix.

The updated state and covariance are given by

$$\hat{X}(k+1|k+1)=\hat{X}(k+1|k)+K(k+1)\gamma(k+1) \tag{22}$$

and

$$P(k+1|k+1)=P(k+1|k)-K(k+1)H(k+1)K'(k+1) \tag{23}$$

respectively.

D. DATA ASSOCIATION

The data association makes the decisions of associating the obtained measurements at k to the established tracks at $k-1$, and to update the track at k. GNN is a 2D assignment that matches the q_k measurement list to the predicted T_{k-1} tracks list by formulating the global optimization problem. The optimization minimizes the overall cost (C) of the measurement-to-track as

$$C=\sum_{i=0}^{q_k}\sum_{t=0}^{T_{k-1}}a(i,t)c(i,t) \tag{24}$$

subjected to

$$\sum_{i=0}^{q_k}a(i,t)c(i,t)=1,\quad t=1,2,\cdots T_{k-1}$$

$$\sum_{t=0}^{T_{k-1}}a(i,t)c(i,t)=1,\quad i=1,2,\cdots q_k$$

The $a(i, t)$ is a binary assignment variable such that

$$a(i,t) = \begin{cases} 1; & \text{measurement } i \text{ associated with target } t \\ 0; & \text{otherwise} \end{cases} \quad (25)$$

Here, all the measurements are indexed in i, and all the tracks are indexed in t to form a 2D matrix. Whereas, c is the cost associated with measurement-to-track; which is equal to the distance between predicted measurement $H\hat{X}(k+1|k)$ and measurement $z_i(k+1)$. The above optimization is solved using munkres algorithm [37].

E. TRACK MANAGEMENT

Total available tracks are classified into tentative tracks and confirmed tracks. Tentative tracks are the ones that have fewer measurements associated than the required number of measurements over a specified time limit. In contrast, confirmed tracks are the tentative tracks that receive more associated measurements and are promoted to be confirmed ones. Also, if an inadequate number of measurements are associated with the tentative track within the specified time, the tentative tracks are deleted. For track maintenance, the logic-based rule [29] is used, given by

1) For track initialization: out of the last N_{init} measurement frames, if at least M_{init} measurements are associated together, then form a track and mark it tentative; otherwise, do nothing.
2) For a tentative track: out of the last N_{tent} measurement frames, if at least M_{tent} measurements are associated to the track, then promote it as confirmed; otherwise, delete the track.
3) For a confirmed track: out of the last N_{conf} measurement frames, if at least M_{conf} measurements are associated to the track, then do nothing; otherwise, delete it.

IV. TRACK TO TRACK ASSOCIATION AND FUSION

The presence of IWCTs produces more tracks at the radar receiver, even though a single target is present in the surveillance region. To determine the actual track originated from a target, it is required to consider more than one radar present in the same surveillance region. Once the tracks are received from all radars, track-to-track association and fusion of tracks are required to identify the true track precisely. Accordingly, this section presents the track-to-track association and track fusion concepts for the generalized scenario, where N number of radars are looking for a target in a surveillance region surrounded by M IWCTs.

A. TRACK-TO-TRACK ASSOCIATION (T2TA)

The N radars have their own number of tracks in the form of target estimate $\hat{x}_i^{\xi_i}$ having their errors are distributed as zero-mean Gaussian with covariance $P_i^{\xi_i}$. The $i = 1, 2, \ldots, N$, represents radar number and $\xi_i = 0, 1, 2, \ldots, T_i$ represents number of tracks that the each radar generates. To find out the tracks corresponds to the same target, it is required to perform the likelihood ratio test, given by

$$\chi(H^1_{\xi_1,\xi_2,\ldots,\xi_N} : H^0_{\xi_1,\xi_2,\ldots,\xi_N}) = \frac{\Lambda(H^1_{\xi_1,\xi_2,\ldots,\xi_N})}{\Lambda(H^0_{\xi_1,\xi_2,\ldots,\xi_N})}, \quad (26)$$

where $\Lambda(H^1_{\xi_1,\xi_2,\ldots,\xi_N})$ represents the likelihood hypothesis of tracks having the common origin, $\Lambda(H^0_{\xi_1,\xi_2,\ldots,\xi_N})$ represents the likelihood hypothesis of tracks having the different origin.

Calculating the likelihood hypothesis of tracks having a common origin is as follows

$$\Lambda(H^1_{\xi_1,\xi_2,\ldots,\xi_N}) = p(\hat{\mathbf{x}}_N^{\xi_N}, \ldots, \hat{\mathbf{x}}_1^{\xi_1} | H^1_{\xi_1,\xi_2,\ldots,\xi_N}). \quad (27)$$

The (27) can also be written conditioned on the track estimate of the first radar, given by

$$\Lambda(H^1_{\xi_1,\xi_2,\ldots,\xi_N}) = p(\hat{\mathbf{x}}_N^{\xi_N}, \ldots, \hat{\mathbf{x}}_2^{\xi_2} | H^1, \hat{\mathbf{x}}_1^{\xi_1}) p(\hat{\mathbf{x}}_1^{\xi_1} | H^1). \quad (28)$$

The $p(\hat{\mathbf{x}}_1^{\xi_1}|H^1)$ is independent of $H^1_{\xi_1,\xi_2,\ldots,\xi_N}$, hence it can be relaxed. Also, it is assumed to be a uniform distribution, which is a valid assumption in the case of a lack of information. i.e.,

$$p(\hat{\mathbf{x}}_1^{\xi_1} | H^1_{\xi_1,\xi_2,\ldots,\xi_N}) = p(\hat{\mathbf{x}}_1^{\xi_1}) = \frac{1}{C}. \quad (29)$$

Substituting (29) into (28) results

$$\Lambda(H^1_{\xi_1,\xi_2,\ldots,\xi_N}) = \frac{1}{C} p(\hat{\mathbf{x}}_N^{\xi_N}, \ldots, \hat{\mathbf{x}}_2^{\xi_2} | H^1, \hat{\mathbf{x}}_1^{\xi_1}). \quad (30)$$

Consider the two radar (i, j) case that has two tracks (ξ_i, ξ_j) as common target origin. Under the Gaussian assumption, if the tracks $\hat{\mathbf{x}}_i^{\xi_i}, \hat{\mathbf{x}}_j^{\xi_j}$ at radar i, and radar j result from the same target, the likelihood function of the two tracks is given by [30]

$$\Lambda(H_{\xi_i,\xi_j}) = \frac{1}{C} \mathcal{N}(\hat{\mathbf{x}}_i^{\xi_i} - \hat{\mathbf{x}}_j^{\xi_j}; 0, P_i^{\xi_i} + P_j^{\xi_j} - P_{i,j}^{\xi_i,\xi_j} - (P_{i,j}^{\xi_i,\xi_j})'), \quad (31)$$

where $\mathcal{N}(\mathbf{x}; \bar{\mathbf{x}}, P)$ represents Gaussian distribution of variable $\mathbf{x}$ with mean and covariance as $\bar{\mathbf{x}}$, P, respectively.

Similar to (31), the generalized likelihood function of all the common tracks (zero error tracks) $\xi_1, \xi_2, \ldots, \xi_N$ for all N radars is defined as

$$\Lambda(H^1_{\xi_1,\xi_2,\ldots,\xi_N}) = \frac{1}{C} \mathcal{N}(\hat{\mathbf{x}}; 0, P). \quad (32)$$

Here

$$\hat{\mathbf{x}} = \left[\tilde{\mathbf{x}}_{21}, \ \tilde{\mathbf{x}}_{31}, \ \ldots, \ \tilde{\mathbf{x}}_{N1}\right]', \quad (33)$$

where $\tilde{\mathbf{x}}_{ij}$ represents the difference of the estimates resulted from the same target at i^{th} and j^{th} radar, given by

$$\tilde{\mathbf{x}}_{ij} = \hat{\mathbf{x}}_i^{\xi_i} - \hat{\mathbf{x}}_j^{\xi_j}. \quad (34)$$

The diagonal elements of P are represented as

$$\begin{aligned} P_{i-1,i-1} &= \mathbb{E}[\tilde{\mathbf{x}}_{i1} \tilde{\mathbf{x}}_{i1}' | H^1_{\xi_1,\xi_2,\ldots,\xi_N}], \\ &= P_1^{\xi_1} + P_i^{\xi_i} - P_{1,i}^{\xi_1,\xi_i} - (P_{1,i}^{\xi_1,\xi_i})' \quad i = 2, \ldots, N \end{aligned} \quad (35)$$

where $\tilde{\mathbf{x}}_{ij}$ is defined in (34).

Off-diagonal elements of P are given by

$$\begin{aligned} P_{i-1,j-1} &= \mathbb{E}[\tilde{\mathbf{x}}_{i1}\tilde{\mathbf{x}}'_{j1}|H^1_{\xi_1,\xi_2,\ldots,\xi_N}], \\ &= P_1^{\xi_1} - P_{1,j}^{\xi_1,\xi_j} - (P_{1,i}^{\xi_1,\xi_i})' + P_{i,j}^{\xi_i,\xi_j}, \quad i,j=2,\ldots,N \end{aligned} \tag{36}$$

Similar to (32), the likelihood hypothesis of tracks having different origins follows the same procedure as above, specified as

$$\begin{aligned} \Lambda(H^0_{\xi_1,\xi_2,\ldots,\xi_N}) &= p(\hat{\mathbf{x}}_N^{\xi_N},\ldots,\hat{\mathbf{x}}_2^{\xi_2}|H^0,\hat{\mathbf{x}}_1^{\xi_1})p(\hat{\mathbf{x}}_1^{\xi_1}|H^0) \\ &= \prod_{i=2}^{N} p(\hat{\mathbf{x}}_i^{\xi_i}|H^0,\hat{\mathbf{x}}_1^{\xi_1})p(\hat{\mathbf{x}}_1^{\xi_1}|H^0) \end{aligned} \tag{37}$$

Similar to (29), the $p(\hat{\mathbf{x}}_1^{\xi_1}|H^0_{\xi_1,\xi_2,\ldots,\xi_N})$ is assumed as diffuse prior, given by

$$p(\hat{\mathbf{x}}_1^{\xi_1}|H^0_{\xi_1,\xi_2,\ldots,\xi_N}) = p(\hat{\mathbf{x}}_1^{\xi_1}) = \frac{1}{C}, \tag{38}$$

whereas, $p(\hat{\mathbf{x}}_N^{\xi_N},\ldots,\hat{\mathbf{x}}_2^{\xi_2}|H^0,\hat{\mathbf{x}}_1^{\xi_1})$ is assumed to follow Poisson distribution in the state space with a spatial density λ. Therefore, substituting (38) into (37) yields

$$\Lambda(H^0_{\xi_1,\xi_2,\ldots,\xi_N}) = \frac{1}{C}\lambda^{N-1}. \tag{39}$$

Finally, from (26), (32), (39), the likelihood ratio test is given by

$$\chi(H^1_{\xi_1,\xi_2,\ldots,\xi_N} : H^0_{\xi_1,\xi_2,\ldots,\xi_N}) = \frac{\mathcal{N}(\hat{\mathbf{x}};0,P)}{\lambda^{N-1}}, \tag{40}$$

For T2TA, define the track-to-track assignment algorithm of assigning the ξ_i tracks that result from N radars representing the same target. For this, the binary assignment variable is defined as

$$\psi_{\xi_1,\xi_2,\ldots,\xi_N} = \begin{cases} 1; & \text{tracks } \xi_1,\xi_2,\ldots,\xi_N \text{ from same} \\ & \text{target} \\ 0; & \text{from different target} \end{cases} \tag{41}$$

The multidimensional (S-D) track-to-track assignment algorithm of finding the most likely hypothesis is the result of the constrained optimization problem given below

$$\min_{\psi_{\xi_1,\xi_2,\ldots,\xi_N}} \sum_{\xi_1=0}^{T_1}\sum_{\xi_2=0}^{T_2}\cdots\sum_{\xi_N=0}^{T_N} c_{\xi_1,\xi_2,\ldots,\xi_N}\psi_{\xi_1,\xi_2,\ldots,\xi_N} \tag{42}$$

subject to

$$\begin{aligned} \sum_{\xi_2=0}^{T_2}\cdots\sum_{\xi_N=0}^{T_N}\psi_{\xi_1,\xi_2,\ldots,\xi_N} &= 1, \quad \xi_1 = 1,2,\ldots,T_1 \\ \sum_{\xi_1=0}^{T_1}\sum_{\xi_3=0}^{T_3}\cdots\sum_{\xi_N=0}^{T_N}\psi_{\xi_1,\xi_2,\xi_3,\ldots,\xi_N} &= 1, \quad \xi_2 = 1,2,\ldots,T_2 \\ &\vdots \\ \sum_{\xi_1=0}^{T_1}\cdots\sum_{\xi_{N-1}=0}^{T_{N-1}}\psi_{\xi_1,\ldots,\xi_{N-1},\xi_N} &= 1, \quad \xi_N = 1,2,\ldots,T_N \end{aligned} \tag{43}$$

and

$$\begin{aligned} \psi_{\xi_1,\ldots,\xi_N} &\in \{0,1\}, \\ \xi_1 &= 0,1,\ldots,T_1, \\ &\vdots \\ \xi_N &= 0,1,\ldots,T_N \end{aligned} \tag{44}$$

The cost function $c_{\xi_1,\xi_2,\ldots,\xi_N}$ in (42) can be calculated as

$$c_{\xi_1,\xi_2,\ldots,\xi_N} = -\ln\chi(H^1 : H^0). \tag{45}$$

where $\chi(H^1 : H^0)$ is the likelihood ratio, given in (40).

B. CORRELATION FREE FUSION

This subsection considers the covariance intersection (CI) method for track-to-track fusion (T2TF). As it is a memoryless algorithm, cross-covariance among the local tracks is not utilized. Two algorithms are considered in the CI method; one is the original CI algorithm, and the other is sampling CI (SCI). The SCI is also considered; because as the number of tracks that need to be fused increases, the original CI becomes computationally demanding.

1) ORIGINAL COVARIANCE INTERSECTION (CI) ALGORITHM

Suppose the T2TA algorithm reveals T_N independent tracks of N radars representing the same target, which needs to be fused, the approximate CI of those N non-Gaussian uncertainties is given by [35]

$$P_{CI}^{-1} = \omega_{T_1}P_{T_1}^{-1} + \omega_{T_2}P_{T_2}^{-1} + \ldots + \omega_{T_N}P_{T_N}^{-1}, \tag{46}$$

where

$$0 \le \omega_{T_i} \le 1 \text{ and } \sum_{T_i=1}^{N}\omega_{T_i} = 1. \tag{47}$$

The fused state estimate is represented as

$$P_{CI}^{-1}\hat{\mathbf{x}}_{CI} = \omega_{T_1}P_{T_1}^{-1}\hat{\mathbf{x}}_{T_1} + \omega_{T_2}P_{T_2}^{-1}\hat{\mathbf{x}}_{T_2} + \ldots + \omega_{T_N}P_{T_N}^{-1}\hat{\mathbf{x}}_{T_N}. \tag{48}$$

For the above (48), a closed form solution for lower dimensional matrix is presented in [38].

2) SAMPLING COVARIANCE INTERSECTION (SCI) ALGORITHM

The fused estimate in the case of SCI method of fusing the T_N independent tracks of N radars representing the same target is given by [35]

$$P_0^{-1} = \sum_{T_i=1}^{N} P_{T_i}^{-1}, \tag{49}$$

$$\hat{\mathbf{x}}_{SCI} = P_0\left(\sum_{T_i=1}^{N} P_{T_i}^{-1}\hat{\mathbf{x}}_{T_i}\right). \tag{50}$$

To prevent the covariance is optimistic, the following procedure is used to adjust the size of the covariance matrix. Generate the S number of random samples $\mathbf{x}_j = \mathcal{N}(0, P_0), j = 1, \ldots, S$. Next find the r_{max} and r_{min} using

$$r_{\max} = \max_{j=1,2,\ldots,S} \frac{\mathbf{x}_j' P_0^{-1} \mathbf{x}_j}{\max\limits_{T_i=1,2,\ldots,N} \hat{\mathbf{x}}_{T_i}' P_{T_i}^{-1} \hat{\mathbf{x}}_{T_i}}, \tag{51}$$

$$r_{\min} = \min_{j=1,2,\ldots,S} \frac{\mathbf{x}_j' P_0^{-1} \mathbf{x}_j}{\max\limits_{T_i=1,2,\ldots,N} \hat{\mathbf{x}}_{T_i}' P_{T_i}^{-1} \hat{\mathbf{x}}_{T_i}}. \tag{52}$$

Finally, set the fused covariance SCI as

$$P_{SCI} = \frac{P_0}{u r_{min} + (1-u) r_{max}}, \quad u \in [0, 1], \tag{53}$$

where u is used to adjust the performance of the SCI algorithm [35].

V. POSTERIOR CRAMER-RAO LOWER BOUND (PCRLB)

In this section, to compare the simulation performance of the proposed framework, the Posterior Cramer-Rao Lower Bound (PCRLB) is considered. The PCRLB is the theoretical lower bound, which quantifies the estimation accuracy [25]. Let $\hat{X}_{k+1}$ be the estimate of the state vector X_{k+1} conditioned on measurement set $z_{1:k+1}$. The PCRLB [39] on the covariance P_{k+1} is the inverse of the Fisher information matrix (FIM) J_{k+1}, given by

$$P_{k+1} \triangleq \mathbb{E}\left[\left(\hat{X}_{k+1} - X_{k+1}\right)\left(\hat{X}_{k+1} - X_{k+1}\right)'\right] \geq J_{k+1}^{-1}. \tag{54}$$

The FIM J_{k+1} can be evaluated recursively by

$$J_{k+1} = D_k^{22} - D_K^{21}(J_k + D_k^{11})^{-1} D_k^{12}, \tag{55}$$

where

$$\begin{aligned} D_k^{11} &= F_k' Q_k^{-1} F_k, \\ D_k^{12} &= D_k^{21} = -F_k' Q_k^{-1}, \\ D_k^{22} &= Q_k^{-1} + J_{z,k+1}. \end{aligned} \tag{56}$$

Here, $J_{z,k+1}$ corresponds to measurement contribution, given by (for brevity, subscript k + 1 for X is omitted here):

$$J_{z,k+1} = b(p_D, \lambda V, g)\left\{[\nabla_X h(X)]' R_{k+1}^{-1} [\nabla_X h(X)]\right\}, \tag{57}$$

where, $b(.)$ is the information reduction factor (IRF), accounting for the reduction of information due to false alarms and the measurements due to IWCTs in the available measurements. Which is a scalar quantity, depends on detection probability (p_D), false alarm density (λ), volume of the surveillance region (V), and gated volume (g). The expansion and the numerical evaluation of IRF is presented in [40]–[42]. The value of IRF $b(.)$ is approximately equal to p_D. The $\nabla_X h(X)$ in (57) is the Jacobian matrix, given by

$$\nabla_X h(X) = \begin{pmatrix} \frac{(x_l^t - x_n^r)}{R_n^l} & 0 & \frac{(y_l^t - y_n^r)}{R_n^l} & 0 \\ \frac{-(y_l^t - y_n^r)}{(R_n^l)^2} & 0 & \frac{(x_l^t - x_n^r)}{(R_n^l)^2} & 0 \end{pmatrix}, \tag{58}$$

where R_n^l is defined in (9).

Using matrix inversion Lemma, using (56), the FIM recursion (55) can deduce to

$$J_{k+1} = \left[Q_k + F_k J_k^{-1} F_k'\right]^{-1} + J_{z,k+1}. \tag{59}$$

The initial value of FIM $J_0 = (P_0)^{-1}$.

In this paper, multiple radars (N) are used to identify the true target, and the information is fused to get a better estimate. So, to compare the estimation accuracy of the fused estimate, there is a need to calculate the fused FIM over the multiple radars. Therefore, the fused PCRLB follows (54) by replacing J with summation of all the FIMs from all the radars, given by

$$\mathbb{E}\left[\left(\hat{X}_{k+1} - X_{k+1}\right)\left(\hat{X}_{k+1} - X_{k+1}\right)'\right] \geq \left\{\sum_{i=1}^{N} J_{k+1}^i\right\}^{-1}, \tag{60}$$

where $J_{k+1}^{(.)}$ for each radar is given in (59). Further, in this paper, the PRMSE is used as quantifying metric; the square root is applied over the positional terms of PCRLB given in (60). Furthermore, in this paper, PCRLB corresponds to square root PCRLB of the positional terms unless specified.

VI. RESULTS AND DISCUSSION

The results and discussion are presented in this section. A single radar case and multiple radar cases are considered to illustrate the ambiguity of target tracking in the presence of IWCTs and to mitigate its effect.

A. SINGLE RADAR CASE

In this case, a single radar, single target, and multiple IWCTs are considered to exemplify the problem of target tracking.

1) SCENARIO GENERATION

The simulation scenario considered is that the radar and IWCTs are assumed to be static in a given surveillance region of 12000 × 12000 with a maximum range at which radar can detect the targets is 12000m. First, the simulations are considered for the case of existence of a single radar present at the origin $[0, 0]'$ and four in-band static transmitters; their locations are presented in TABLE 1 (near-geometry refers to nearby IWCTs to radar, and far-geometry refers to IWCTs are located far from radar). Only a single target is considered with constant velocity (CV) model; the initial state of the target is

$$\begin{aligned} X(0) &= [x, \dot{x}, y, \dot{y}]' \\ &= [1000, 30, 1000, 0]' \end{aligned} \tag{61}$$

TABLE 1. In-band wireless communication transmitters location for single radar case.

	near-geometry		far-geometry	
In-band transmitter	x (m)	y (m)	x (m)	y (m)
1	300	1700	6000	3000
2	1500	1500	500	8000
3	2000	1500	5000	500
4	1700	1800	3000	5000

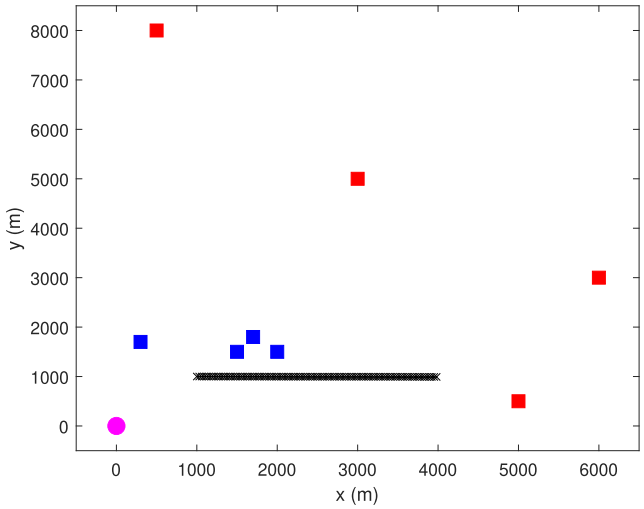

FIGURE 3. Scenario generation for a single radar case, where the circle indicates radar location, squares represent in-band transmitters (red color for far-geometry and blue color for the near-geometry scenario), and the black line replicates the target trajectory.

The target protuberance in both position and velocity components is modeled as process noise, follows additive white Gaussian pdf, and is considered as

$$v=[\mathcal{N}(0,0.05^2),\mathcal{N}(0,0.02^2),\mathcal{N}(0,0.05^2),\mathcal{N}(0,0.02^2)]', \tag{62}$$

here, $\mathcal{N}(\mu,\sigma^2)$ represents Gaussian pdf with mean μ and standard deviation σ.

The target starts at 1s and ends at 100s. The sampling time of the radar is 1s. On the other hand, the radar receives the range and azimuth measurements and are corrupted with the additive Gaussian noise, and the measurement noise vector is given by

$$w=[\mathcal{N}(0,10^2\text{ m}),\mathcal{N}(0,0.03^2\text{ rad})]' \tag{63}$$

2) TRACKER

The EKF framework is used in the tracker; the tunable parameters like process noise covariance and the measurement noise covariance in (17) and (21) are tuned to

$$Q=\text{diag}([0.05^2\ 0.02^2\ 0.05^2\ 0.02^2]) \tag{64}$$

$$R=\text{diag}([10^2\ 0.03^2]) \tag{65}$$

For track initialization, single point track initialization method [43] is used with maximum velocity, $V_{\max}=30$ m/s.

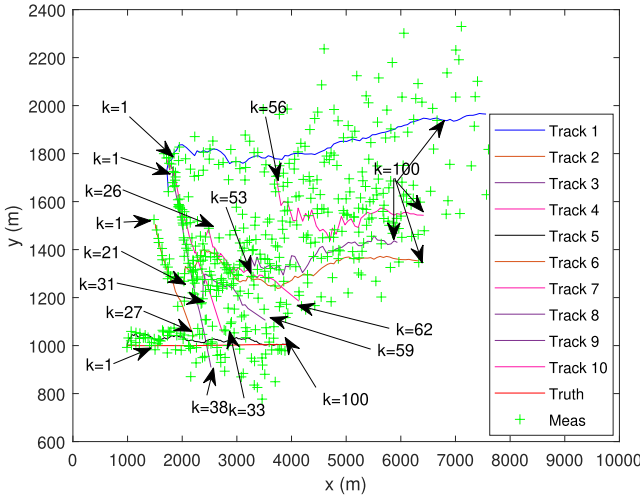

FIGURE 4. Tracking in state space for near-geometry scenario.

A GNN association-based EKF with a CV model is deployed in the tracking framework. A gating technique is used to validate the measurements, which follows a chi-square distribution $\chi_d^2(1-t_p)$, where d is the degree of freedom and t_p is the tail probability. Here, the logic-based track maintenance [44] is opted to confirm or delete the tracks. Once the tracks are initialized, based on the number of measurements being assigned in the given frames, the tracks are either confirmed or deleted. The track confirmation is based on $7/10$ logic, and track termination/deletion is based on $4/10$ logic.

In a single radar case, near and far geometry scenarios are examined to evaluate the tracking performance. For the near-geometry scenario, the IWCTs are near to both the radar and target; the simulation scenario is shown in Figure 3. After the measurements are processed with the GNN tracker, it is observed from Figure 4 that ten tracks are reported by the tracker, in which two tracks are full-length tracks, and the rest are partial tracks. Since the target is moving in the given surveillance, the acquired measurements change over time and may not fit in the predefined models like CV, CA, and CT. This wrong measurement to track association leads to track breakages and, in turn, results in track termination over time. It is observed that track-2, track-3, and track-4 are terminated at $k=27$, $k=38$, and $k=33$ respectively. Whereas track-1 is the false track that occurred throughout the simulation. Interestingly, the track due to monostatic returns is preserved and is reported as a full track with the ID of track-5. The unassociated measurements corresponding to terminated tracks give birth to new tracks as track-6, track-7, track-8. The track-6 evolved at $k=21$ and continued till $k=100$, whereas track-7, track-8 are evolved at $k=26$, $k=31$ and continued till $k=62$, $k=59$ and then terminated. They gave birth to new tracks (track-9, track-10) that evolved at $k=53$, $k=56$ and are confirmed till the end. It is noticed that track-2 and track-6 belong to the same track. Also, track-3, track-8, and track-9 belong to the same track. Further, track-4, track-7, and track-10 belong to the same track and correspond

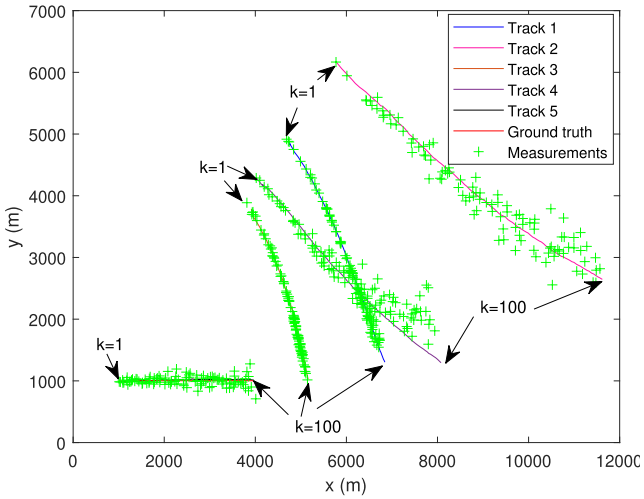

FIGURE 5. Tracking in state space for far-geometry scenario.

to the same in-band transmitter. Sometimes, the overlapping of tracks is due to the last five predictions of the tracks before termination. Hence, the presence of IWCTs near both the radar and target will result in more tracks with track breakages.

The simulation scenario for the far-geometry case, where IWCTs are located far from the target and radar, is depicted in Figure 3. In this scenario, it is observed from Figure 5 that the GNN tracker has reported five tracks. All the reported five tracks are of full length i.e., from $k = 1$ to $k = 100$. Among the five tracks, only track-5 is the true track; the rest corresponds to the measurements arising from the IWCTs. Compared to the near geometry case, the track reports and track breakages are less. Although, in both cases, IWCTs produce false tracks, making the tracker ambiguous to decide which track belongs to the true target. Further, the confirmed false tracks report that more targets are present in the given surveillance region. It is hard to distinguish the true track from all the available tracks. Hence, in this paper, it is proposed to use the local tracks obtained from multiple radars and resolve the ambiguous tracks.

B. MULTIPLE RADAR CASE

This subsection examines the case of distributed radars and in-band transmitters. Initially, two radars (R1, R2) and four IWCTs (C1, C2, C3, and C4) are considered in the surveillance region. Next, this case is extended for four radars (R1, R2, R3, R4). It is assumed that both radars and IWCTs are static. In contrast, the target is dynamic and follows the CV model. The locations of both radars and in-band communication transmitters are tabulated in Table 2 and are depicted in Figure 6. Since the distributed tracking followed by fusion is deployed, each radar provides its local tracks. The track-to-track association is performed on the local tracks as presented in Section IV-A. In this process, the overall optimization provides the tuples of tracks. Among them, only one track is quantified by performing a chi-square distribution test. Once

TABLE 2. The locations of radars and in-band wireless communication transmitters for multiple radar case.

	Radar (R)		In-band transmitter (C)	
S.No.	x (m)	y (m)	x (m)	y (m)
1	5000	2000	500	500
2	500	2000	500	8000
3	700	9000	5000	500
4	6000	7000	6000	8000

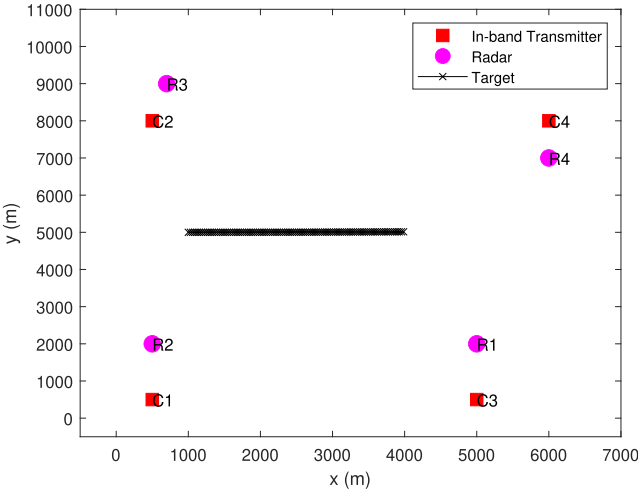

FIGURE 6. Scenario generation for multiple radar case.

the true track associated with each radar is known, these quantified local tracks are fused at the fusion center to yield a global estimate. Various correlation-free fusion algorithms are presented in Section IV-B.

Figure 7 shows the obtained local tracks of R1 and R2 sensors in a clean environment (unity target detection probability and zero false alarm density). It is observed that even though there exists a single target in the surveillance, multiple tracks result at each sensor. Only two local tracks represent the actual target tracks pertaining to sensor-1 and sensor-2. The rest of the tracks fall apart within the surveillance due to the additional time delay introduced by the IWCTs. Further, if the IWCTs are co-located in the vicinity of radar, then the false local track corresponding to IWCTs also appears near the true trajectory locations. In this case, due to the spatial deployment of IWCTs, it is observed that the local tracks are spatially separated. It is worth noting that one local track from the track set of each radar represents the true target. For the case of low target detection probability, the above condition of one local track from the target set becomes unrealistic. In addition, with the T2TA, the overlapped tracks appeared as a tuple. Even with the increase in the number of radars, a single track from the track set represents the actual target track, and it is easily be quantified by using T2TA.

Figures 8-10 show the PRMSE and the corresponding achievable lower bound (PCRLB) of the fused tracks and the associated radar tracks for two radar case by choosing different p_D and false alarm density. The ellipsoidal

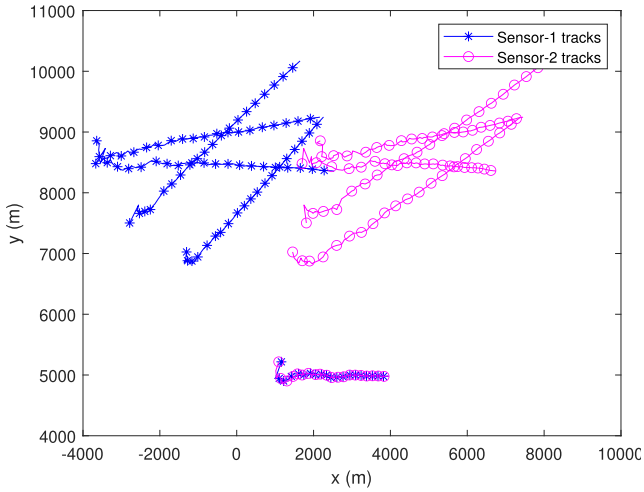

FIGURE 7. Illustration of local tracks pertain to R1 and R2 with unity p_D and zero false alarm density.

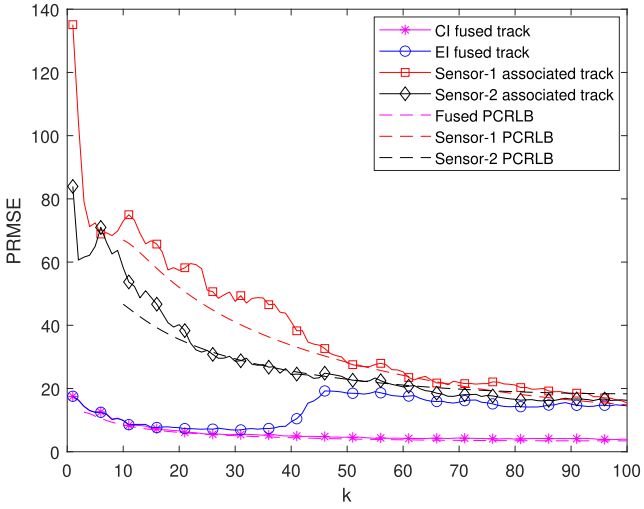

FIGURE 8. PRMSE of two radar case with unity p_D and zero false alarm density.

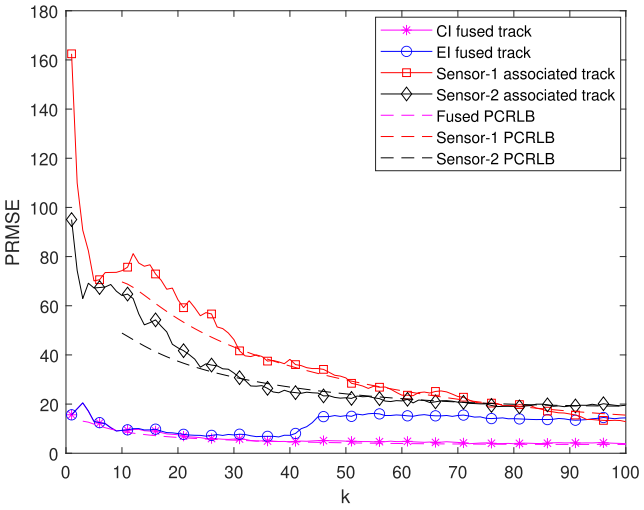

FIGURE 9. PRMSE of two radar case with p_D 0.9 and false alarm density as 1×10^{-7}.

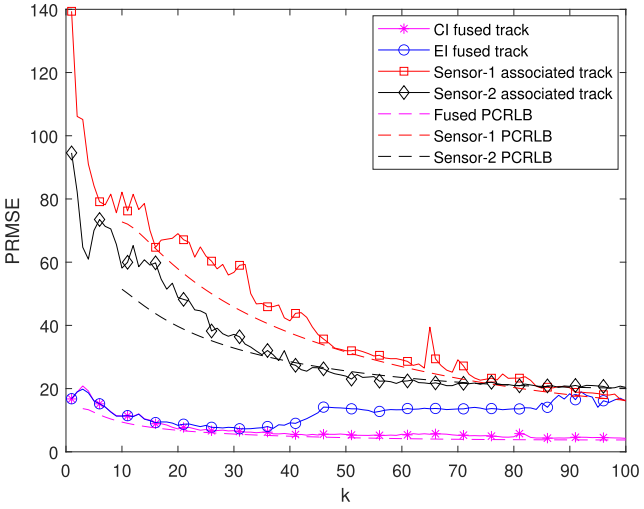

FIGURE 10. PRMSE of two radar case with p_D 0.8 and false alarm density as 1×10^{-7}.

intersect (EI) [33] and CI fusion methods have been used for a two radars case to find the fused state estimates. The ellipsoidal method uses the mutual information-based mean and covariance, which are derived using two initial estimates, to calculate the final fused mean and covariance [33]. On the other hand, CI uses trace or determinant minimization to determine the fused covariance. This minimization becomes a nonlinear convex optimization problem. The solution can be found using the well-known polynomial root-finding problem, which allows closed-form solutions to find the final fused covariance.

In particular, Figure 8 shows the PRMSE for clean environment. Since the tracker is initialized with a one-point initialization, with $V_{max} = 30$ and converted measurement, the PRMSE is very high at $k = 0$. During the time period of $k \in [1, 20]$, the filter settles its covariance, and it is visualized that the PRMSE is decreasing over time. After a certain time $k = 40$, the filter is settled, and settled PRMSE values are observed. Interestingly, the fused estimate with EI agrees with the CI method till $k = 40$, and its performance begins to degrade after a few scans. This is due to the unsettled covariance of any of the tracks. It is the main drawback of the ellipsoidal method. The fusion with the CI method provides improved performance compared to the EI and has less fused PRMSE values.

The Figure 9 and 10 shows the PRMSE of the two radar case having false alarm density 1×10^{-7} with p_D as 0.9 and 0.8, respectively. It is observed from Figure 9 that the PRMSE of the associated tracks has a higher value in comparison with the Figure 8. It is because the decrease in p_D increases the measurement ambiguity. Since the track termination rule follows 4/10, it indicates that a continuous track exists even though there is an absence of measurement for three consecutive scans. During the unavailability of measurement in

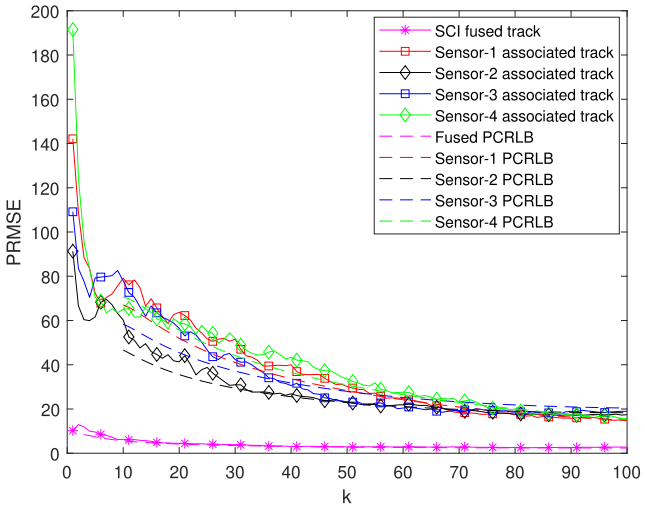

FIGURE 11. PRMSE of four radar case with unity p_D and zero false alarm density.

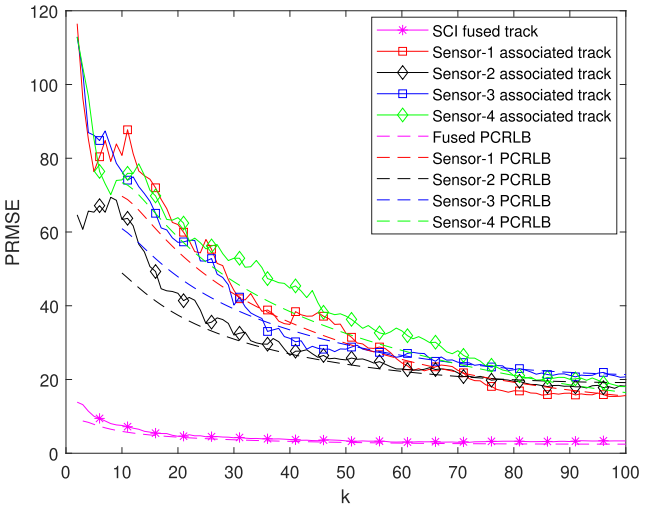

FIGURE 12. PRMSE of four radar case with p_D 0.9 and false alarm density as 1×10^{-7}.

a given scan, the tracker uses the predicted estimate as an updated estimate. The prediction state cannot withstand the error due to the process noise, which in turn raises the PRMSE values for these scans. In the presence of measurement origin uncertainty, the continuous track can be achieved with degraded accuracy by increasing the track termination rule. Even though PRMSE of the associated tracks has a noticeable degrade with the decrease in p_D, the fused estimate has less performance degradation. Similar statements hold true for Figure 10. Further, from Figures 8-10, it is noted that the estimation PRMSE values are in agreement with the PCRLB values.

Generally, the fusion of individual local estimates leads to a better estimate. Assuming that four radars (R1, R2, R3, R4) are present in a surveillance region, the Figures 11-13 show the PRMSE of the four radar case for different values of p_D and p_{FA}. The PRMSE is also quantified with PCRLB. The locations of radars are provided in Table 2, and are depicted in Figure 6. In contrast to two radar case, here, the SCI method is deployed to fuse the associated tracks. Because the EI is limited to two sources, the CI is computationally expensive for more sources. In contrast to CI, the SCI first fuses the local track estimates with an assumption that they are independent. After that, the covariance size of the fused track estimate is modified through a sampling process. The fuser weight parameter plays a critical role in estimating the mean in SCI. For a given unity fuser weight, the fuser is pessimistic. Whereas, for a zero fuser weight, the fuser is optimistic. The fuser weight of 0.5 provides the best consistency [35]. Henceforth, in this simulation, the fuser weight value is set to 0.5.

It is observed from Figures 11-13 that, since a single point initialization is used [45], the PRMSE for initial time stamps is higher. Once the covariance of the filter is settled, the PRMSE decreases with the increase in time. Further, the PRMSE values of Figure 12 and 13 are higher when

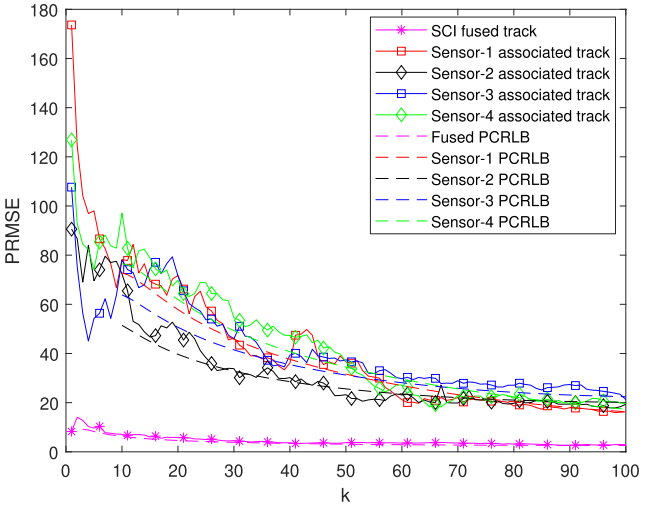

FIGURE 13. PRMSE of four radar case with p_D 0.8 and false alarm density as 1×10^{-7}.

compared to the clean environment, shown in Figure 11. The decrease in p_D increases the measurement ambiguity at the radar, which in turn increases the PRMSE. Besides, it is worth noting from Figures 11-13 that, the four radar fusion estimate provides improved PRMSE compared to the two radar case of Figures 8-10. Also, from Figures 8-13, it is noted that, the increase in the number of radars considered for fusion further improves the estimation PRMSE values and meets with the fused PCRLBs.

To clearly show the efficacy of fusing the information from multiple radars, Figure 14 shows the PRMSE of the four radar case and two radar case for different values of p_D. Further, to clearly distinguish the difference in PRMSE, Figure 14 is plotted with X-axis on a linear scale and Y-axis on a logarithmic scale. It is worth noting that the PRMSE of the four radar fusion estimates is always less when compared to two radar fusion for various values of p_D. For example, for

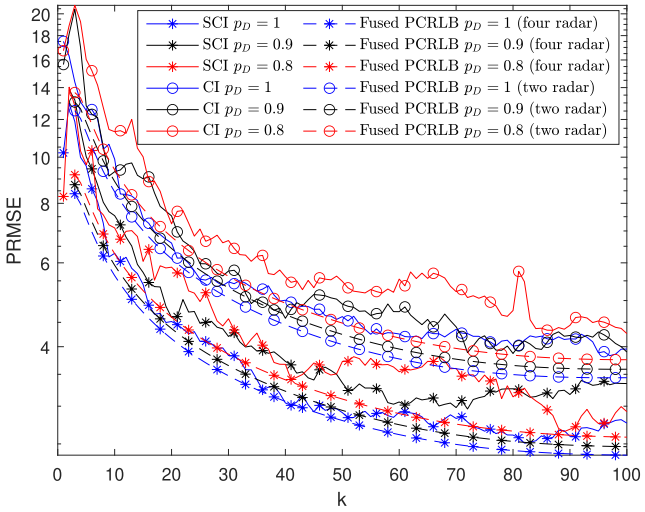

FIGURE 14. Comparison of PRMSE for four radar and two radar case with varying p_D.

$p_D = 0.9$, the four radar case PRMSE is lower than the two radar case and holds true for other values of p_D. The four radar case fusion provides a two-fold performance compared to two radar case fusion. Therefore, the deployment of more radars not only benefits the elimination of false tracks but also provides improved target tracking performance. Further, fusing the information from more sensors improves the estimation accuracy, with PRMSE values much closer to PCRLBs.

VII. CONCLUSION

This paper presents a new measurement model for the RadComm spectrum sharing scenario and evaluates the target tracking performance. The new measurement model incorporates the radar returns and returns due to in-band wireless communication transmitters (IWCTs). Due to the presence of IWCTs, a huge number of measurements are available in a given scan. For the obtained measurement set, the measurement to track association is carried out using GNN, whereas, for the filtering performance, EKF is considered in the tracker. The GNN-EKF based tracker is used to evaluate the tracking performance with metrics like false tracks, track breakages, and PRMSE. To provide the theoretical lower bound on the estimation accuracy, the PCRLB is considered for the proposed framework. A single radar and multiple radar cases are considered in the simulation scenario. Two different geometry frameworks are considered in a single radar case, where IWCTs are located near and far from the target and radar. The simulation results demonstrated that, in the presence of IWCTs, a huge number of tracks and track breakages are reported for the near geometry case. On the other hand, a few tracks are reported in the far geometry case. However, both cases have reported false tracks, which creates a delusion that more targets are present in the given surveillance. Multiple radar case is employed to eliminate the false tracks and determine the true target track. All the tracks reported by the multiple radars are first associated to find the true target track from each radar. Once the true target track of each radar is identified, T2TF is performed to determine an improved estimate of the true target track. In a RadComm spectrum sharing, for the multiple radar case, simulation results reveal that by performing T2TA and T2TF, the true target track can be estimated with enhanced accuracy. It is evident from the results that the RMSE of the target estimates agrees with PCRLBs. This paper identifies the true track of the target by considering the multiple radars. Further, it eliminates the information from IWCTs in a RadComm spectrum sharing scenario. In the future, one can develop more sophisticated target tracking algorithms, where a single radar alone can identify the true targets in the RadComm spectrum sharing scenario. This work can also be extended by incorporating the information/ measurements received from surrounding IWCTs and improving the target estimation performance.

ACKNOWLEDGMENT

The authors Gunnery Srinath and Bethi Pardhasaradhi thank Prof. T. Kirubarajan and Dr. R. Tharmarasa for providing valuable inputs during their stay at the ETF Laboratory, McMaster University, Canada, as a Visiting Research Scholar, from 2018 to 2019.

REFERENCES

[1] D. Kutscher, H. Lundqvist, and F. G. Mir, "Congestion exposure in mobile wireless communications," in *Proc. IEEE Global Telecommun. Conf. GLOBECOM*, Dec. 2010, pp. 1–6.
[2] G. Forecast, "Cisco visual networking index: Global mobile data traffic forecast update, 2017–2022," *Update*, vol. 2017, p. 2022, Feb. 2019.
[3] B. Paul, A. R. Chiriyath, and D. W. Bliss, "Survey of RF communications and sensing convergence research," *IEEE Access*, vol. 5, pp. 252–270, 2017.
[4] S. D. Blunt and E. S. Perrins, Eds., *Radar and Communication Spectrum Sharing* (Radar, Sonar & Navigation). London, U.K.: Institution of Engineering and Technology, 2018.
[5] J. A. Zhang, F. Liu, C. Masouros, R. W. Heath, Z. Feng, L. Zheng, and A. Petropulu, "An overview of signal processing techniques for joint communication and radar sensing," *IEEE J. Sel. Topics Signal Process.*, vol. 15, no. 6, pp. 1295–1315, Nov. 2021.
[6] J. A. Zhang, M. L. Rahman, K. Wu, X. Huang, Y. J. Guo, S. Chen, and J. Yuan, "Enabling joint communication and radar sensing in mobile networks—A survey," 2020, *arXiv:2006.07559*.
[7] N. Nartasilpa, D. Tuninetti, N. Devroye, and D. Erricolo, "Let's share CommRad: Effect of radar interference on an uncoded data communication system," in *Proc. IEEE Radar Conf. (RadarConf)*, May 2016, pp. 1–5.
[8] M. Bica and V. Koivunen, "Radar waveform optimization for target parameter estimation in cooperative radar-communications systems," *IEEE Trans. Aerosp. Electron. Syst.*, vol. 55, no. 5, pp. 2314–2326, Oct. 2019.
[9] A. Hassanien, M. G. Amin, Y. D. Zhang, and F. Ahmad, "Signaling strategies for dual-function radar communications: An overview," *IEEE Aerosp. Electron. Syst. Mag.*, vol. 31, no. 10, pp. 36–45, Oct. 2016.
[10] C. Sahin, J. Jakabosky, P. M. McCormick, J. G. Metcalf, and S. D. Blunt, "A novel approach for embedding communication symbols into physical radar waveforms," in *Proc. IEEE Radar Conf. (RadarConf)*, May 2017, pp. 1498–1503.
[11] J. Qian, M. Lops, L. Zheng, X. Wang, and Z. He, "Joint system design for coexistence of MIMO radar and MIMO communication," *IEEE Trans. Signal Process.*, vol. 66, no. 13, pp. 3504–3519, Jul. 2018.
[12] D. W. Bliss, "Cooperative radar and communications signaling: The estimation and information theory odd couple," in *Proc. IEEE Radar Conf.*, May 2014, pp. 50–55.
[13] A. R. Chiriyath and D. W. Bliss, "Effect of clutter on joint radar-communications system performance inner bounds," in *Proc. 49th Asilomar Conf. Signals, Syst. Comput.*, Nov. 2015, pp. 1379–1383.

[14] B. Paul and D. W. Bliss, "Extending joint radar-communications bounds for FMCW radar with Doppler estimation," in *Proc. IEEE Radar Conf. (RadarCon)*, May 2015, pp. 89–94.
[15] T. Tian, T. Zhang, L. Kong, G. Cui, and Y. Wang, "Mutual information based partial band coexistence for joint radar and communication system," in *Proc. IEEE Radar Conf. (RadarConf)*, Apr. 2019, pp. 1–5.
[16] D. P. Zilz and M. R. Bell, "Statistical modeling of wireless communications interference and its effects on adaptive-threshold radar detection," *IEEE Trans. Aerosp. Electron. Syst.*, vol. 54, no. 2, pp. 890–911, Apr. 2018.
[17] D. P. Zilz and M. R. Bell, "Optimal linear detection of signals in cyclostationary, linearly modulated, digital communications interference," *IEEE Trans. Aerosp. Electron. Syst.*, vol. 55, no. 3, pp. 1123–1145, Jun. 2019.
[18] Q. Zhang, X. Wang, Z. Li, and Z. Wei, "Design and performance evaluation of joint sensing and communication integrated system for 5G mmWave enabled CAVs," *IEEE J. Sel. Topics Signal Process.*, vol. 15, no. 6, pp. 1500–1514, Nov. 2021.
[19] A. Tang, S. Li, and X. Wang, "Self-interference-resistant IEEE 802.11 ad-based joint communication and automotive radar design," *IEEE J. Sel. Topics Signal Process.*, vol. 15, no. 6, pp. 1484–1499, 2021.
[20] C. G. Tsinos, A. Arora, S. Chatzinotas, and B. Ottersten, "Joint transmit waveform and receive filter design for dual-function radar-communication systems," *IEEE J. Sel. Topics Signal Process.*, vol. 15, no. 6, pp. 1378–1392, Nov. 2021.
[21] T. Tian, T. Zhang, G. Li, and T. Zhou, "Mutual information-based power allocation and co-design for multicarrier radar and communication systems in coexistence," *IEEE Access*, vol. 7, pp. 159300–159312, 2019.
[22] B. Wang, R. Xie, H. Xu, J. Zhang, H. Han, Z. Zhang, L. Liu, and J. Li, "Target localization and tracking using an ultra-wideband chaotic radar with wireless synchronization command," *IEEE Access*, vol. 9, pp. 2890–2899, 2021.
[23] A. Martone and M. Amin, "A view on radar and communication systems coexistence and dual functionality in the era of spectrum sensing," *Digit. Signal Processing*, vol. 119, Dec. 2021, Art. no. 103135.
[24] Y. Bar-Shalom, X. R. Li, and T. Kirubarajan, *Estimation With Applications to Tracking and Navigation: Theory Algorithms and Software*. Hoboken, NJ, USA: Wiley, 2004.
[25] Y. Bar-Shalom, P. K. Willett, and X. Tian, *Tracking Data Fusion*, vol. 11. Storrs, CT, USA: YBS Publishing, 2011.
[26] A. Sinha, Z. Ding, T. Kirubarajan, and M. Farooq, "Track quality based multitarget tracking approach for global nearest-neighbor association," *IEEE Trans. Aerosp. Electron. Syst.*, vol. 48, no. 2, pp. 1179–1191, Apr. 2012.
[27] Y. Bar-Shalom, F. Daum, and J. Huang, "The probabilistic data association filter," *IEEE Control Syst.*, vol. 29, no. 6, pp. 82–100, Dec. 2009.
[28] S. S. Blackman, "Multiple hypothesis tracking for multiple target tracking," *IEEE Aerosp. Electron. Syst. Mag.*, vol. 19, no. 1, pp. 5–18, Jan. 2004.
[29] X. Jiang, K. Harishan, R. Tharmarasa, T. Kirubarajan, and T. Thayaparan, "Integrated track initialization and maintenance in heavy clutter using probabilistic data association," *Signal Process.*, vol. 94, pp. 241–250, Jan. 2014.
[30] Y. Bar-Shalom, "On the track-to-track correlation problem," *IEEE Trans. Autom. Control*, vol. AC-26, no. 2, pp. 571–572, Apr. 1981.
[31] S. Duncan and S. Sameer, "Approaches to multisensor data fusion in target tracking: A survey," *IEEE Trans. Knowl. Data Eng.*, vol. 18, no. 12, pp. 1696–1710, Dec. 2006.
[32] M. A. Bakr and S. Lee, "Distributed multisensor data fusion under unknown correlation and data inconsistency," *Sensors*, vol. 17, no. 11, p. 2472, Oct. 2017. [Online]. Available: https://www.mdpi.com/1424-8220/17/11/2472
[33] J. Sijs, M. Lazar, and P. P. J. V. D. Bosch, "State fusion with unknown correlation: Ellipsoidal intersection," in *Proc. Amer. Control Conf.*, Jun. 2010, pp. 3992–3997.
[34] L. Chen, P. O. Arambel, and R. K. Mehra, "Estimation under unknown correlation: Covariance intersection revisited," *IEEE Trans. Autom. Control*, vol. 47, no. 11, pp. 1879–1882, Nov. 2002.
[35] X. Tian, Y. Bar-Shalom, and G. Chen, "A no-loss covariance intersection algorithm for track-to-track fusion," *Proc. SPIE*, vol. 7698, Apr. 2010, Art. no. 76980S.
[36] M. A. Richards, J. A. Scheer, and W. A. Holm, Eds., *Principles of Modern Radar: Basic Principles* (Radar, Sonar & Navigation). London, U.K.: Institution of Engineering and Technology, 2010. [Online]. Available: https://digital-library.theiet.org/content/books/ra/sbra021e
[37] F. Bourgeois and J.-C. Lassalle, "An extension of the Munkres algorithm for the assignment problem to rectangular matrices," *Commun. ACM*, vol. 14, no. 12, pp. 802–804, Dec. 1971.
[38] M. Reinhardt, B. Noack, and U. D. Hanebeck, "Closed-form optimization of covariance intersection for low-dimensional matrices," in *Proc. 15th Int. Conf. Inf. Fusion*, Jul. 2012, pp. 1891–1896.
[39] P. Tichavsky, C. H. Muravchik, and A. Nehorai, "Posterior Cramer–Rao bounds for discrete-time nonlinear filtering," *IEEE Trans. Signal Process.*, vol. 46, no. 5, pp. 1386–1396, May 1998.
[40] M. L. Hernandez, A. Farina, and B. Ristic, "PCRLB for tracking in cluttered environments: Measurement sequence conditioning approach," *IEEE Trans. Aerosp. Electron. Syst.*, vol. 42, no. 2, pp. 680–704, Apr. 2006.
[41] T. Kirubarajan, H. Chen, and Y. Bar-Shalom, "Parameter estimation and the CRLB with uncertain origin measurements," *Methodol. Comput. Appl. Probab.*, vol. 3, no. 4, pp. 387–410, 2001.
[42] H. Meng, M. Hernandez, Y. Liu, and X. Wang, "Computationally efficient PCRLB for tracking in cluttered environments: Measurement existence conditioning approach," *IET Signal Process.*, vol. 3, no. 2, pp. 133–149, Mar. 2009.
[43] D. Musicki and T. L. Song, "Track initialization: Prior target velocity and acceleration moments," *IEEE Trans. Aerosp. Electron. Syst.*, vol. 49, no. 1, pp. 665–670, Jan. 2013.
[44] X. He, R. Tharmarasa, T. Kirubarajan, and T. Thayaparan, "A track quality based metric for evaluating performance of multitarget filters," *IEEE Trans. Aerosp. Electron. Syst.*, vol. 49, no. 1, pp. 610–616, Jan. 2013.
[45] M. Mallick and B. L. Scala, "Comparison of single-point and two-point difference track initiation algorithms using position measurements," *Acta Autom. Sinica*, vol. 34, no. 3, pp. 258–265, 2008.

GUNNERY SRINATH (Graduate Student Member, IEEE) received the B.Tech. degree in electronics and communication engineering from Jawaharlal Nehru Technological University, Anantapur, Andhra Pradesh, India, in 2013, and the M.Tech. degree in digital communication from the ABV-IIITM, Gwalior, Madhya Pradesh, India, in 2016. He is currently pursuing the Ph.D. degree in electronics and communication engineering with the National Institute of Technology Karnataka (NITK), Surathkal, Mangalore, Karnataka, India. From 2018 to 2019, he was a Visiting Ph.D. Student with the Estimation, Tracking and Fusion Research Laboratory, McMaster University, Hamilton, ON, Canada. His research interests include cognitive radio, radar signal processing, radar and communication system spectrum sharing, and target tracking.

BETHI PARDHASARADHI (Member, IEEE) received the B.Tech. degree in electronics and communication engineering from Jawaharlal Nehru Technological University Kakinada (JNTUK), Kakinada, Andhra Pradesh, India, in 2014, and the M.Tech. degree in VLSI design from the ABV-Indian Institute of Information Technology and Management at Gwalior (ABV-IIITM), Gwalior, Madhya Pradesh, India, in 2016. He is currently pursuing the Ph.D. degree with the National Institute of Technology Karnataka (NITK), Surathkal, Karnataka, India. He was a Visiting Ph.D. Scholar at the ETF Laboratory, McMaster University, Canada, under the supervision of Prof. T. Kirubarajan, from 2018 to 2019. His research interests include intentional interference in navigation, target tracking, and information fusion. He was a recipient of Sir C. V. Raman Award from the Institution of Engineering and Technology (IET) for Outstanding Academics and Research.

PRASHANTHA KUMAR H. received the M.Tech. degree in digital electronics and communication from the MIT Manipal, Karnataka, India, in 2001, and the Ph.D. degree in electronics and communication engineering from the National Institute of Technology Karnataka (NITK), Surathkal, Karnataka, in 2012. He was an Assistant Professor for seven years at the Department of Electronics and Communication Engineering, MIT Manipal. Since 2013, he has been with the National Institute of Technology Karnataka, Surathkal, as an Assistant Professor. He is a Subject Expert in error control coding, wireless communication, signal processing for communication, and RF microelectronics. He is the author of *MATLAB/Simulink for Digital Signal Processing* (Seoul, South Korea, Hongrung Publishing Company) with Prof. Won Y. Yang.

PATHIPATI SRIHARI (Senior Member, IEEE) received the B.Tech. degree in electronics and communication engineering from Sri Venkateswara University, the master's degree in communications engineering and signal processing from the University of Plymouth, Plymouth, U.K., and the Ph.D. degree in radar signal processing from Andhra University, in 2012. He worked as a Visiting Assistant Professor at McMaster University, Hamilton, ON, Canada, in 2014. He is currently working as an Assistant Professor with the National Institute of Technology Karnataka, Surathkal, India. His research interests include radar target tracking, radar waveform design, and efficient DSP algorithms for radar applications. He is a Senior Member of ACM, a fellow of IETE, and a member of IEICE, Japan. He has received the 2010 IEEE Asia Pacific Outstanding Branch Counselor Award and the Young Scientist Award from the Department of Science and Technology (DST), New Delhi, for carrying out the sponsored research project entitled "Development of efficient target tracking algorithms in the presence of ECM."